

Discretization of Structured Bosonic Environments at Finite Temperature by Interpolative Decomposition: Theory and Application

Hideaki Takahashi* and Raffaele Borrelli*

DISAFA, University of Torino, Grugliasco I10095, Italy

E-mail: hideaki.takahashi@unito.it; raffaele.borrelli@unito.it

Abstract

We present a comprehensive theory for a novel method to discretize the spectral density of a bosonic heat bath, as introduced in [H. Takahashi and R. Borrelli, *J. Chem. Phys.* **161**, 151101 (2024)]. The approach leverages a low-rank decomposition of the Fourier-transform relation connecting the bath correlation function to its spectral density. By capturing the time, frequency, and temperature dependencies encoded in the spectral density-autocorrelation function relation, our method significantly reduces the degrees of freedom required for simulating open quantum system dynamics. We benchmark our approach against existing methods and demonstrate its efficacy through applications to both simple models and a realistic electron transfer process in biological systems. Additionally, we show that this new approach can be effectively combined with the tensor-train formalism to investigate the quantum dynamics of systems interacting with complex non-Markovian environments. Finally, we provide a perspective on the selection and application of various spectral density discretization techniques.

1 Introduction

The study of dynamical properties of quantum systems interacting with their environments is of fundamental importance across multiple disciplines, including organic electronics,^{1,2} biological systems,³⁻⁶ and quantum information theory.⁷ Key processes such as exciton and charge transport in organic materials and decoherence in quantum systems are strongly influenced by environmental degrees of freedom.

Typically, these studies involves coupling the system of interest to bosonic or fermionic environments through a linear coupling and assuming the reservoirs are initially in thermal equilibrium. The dynamical properties of these reservoirs are encoded in the spectral density (SD) function, which describe the intensity of the noise induced by the bath oscillator at a give frequency, that is the strength of the system-bath coupling.^{8,9}

Effective approaches for simulating the dynamics of this class of models include, among others, basis set methods—such as the multilayer multiconfiguration time-dependent Hartree (ML-MCTDH)¹⁰ method, time-dependent density matrix renormalization group (TD-DMRG)¹¹ and thermo field dynamics in tensor-train format (TFD-TT)^{6,12-14}—influence-functional based methods—such as the quasi-adiabatic propagator path integral (QUAPI)^{15,16} and hierarchical equations of motion (HEOM)¹⁷⁻¹⁹—and chain mapping approaches.²⁰⁻²⁴

Many of these methods often requires the mapping of the continuous SD into a discrete system-bath Hamiltonian. Several discretization procedures have been proposed for this purpose.²⁵ Equispaced discretization is a very simple method, and has been utilized in several studies,^{4,26} despite its inherent limitations. Logarithmic discretization²⁷⁻²⁹ has been developed to specifically tackle the low-frequency components of Ohmic and sub-Ohmic SDs. Makri³⁰ has first devised a discretization procedure in which the frequency domain is split into sub-intervals equally contributing to the reorganization energy. This procedure, which we will refer to as mode density method (MDM), has been frequently used in the past for the study of model systems³¹ as well as for realistic spectral densities.³² Alternatively, Gauss quadrature can be used to integrate the bath hybridization function, resulting in a discrete representation of the BCF. In particular, it has been shown that using

the SD as a weight function for the quadrature can significantly improve frequency sampling. This approach is referred to as Bath-Spectral-Density-Orthogonal (BSDO) method.^{33,34}

Yet, developing a general method that can provide an optimal number of frequencies and their relative couplings, tailored to a specific temperature, simulation time, and desired accuracy remains an open challenge. To tackle this problem, Takahashi and Borrelli³⁵ recently introduced a methodology inspired by studies on compressing imaginary-time Green's functions.^{36–39} This new approach uses the low-rank representation of the Fourier-transform relationship between the SD and the bath correlation function (BCF), which captures temporal environmental fluctuations, via Interpolative Decomposition (ID) theory.^{40–43}

In this study, we present an in-depth theoretical and computational study of the features and performances of this methodology and benchmark it against existing techniques. To illustrate its efficacy, we apply it to both simplified model systems and a realistic electron transfer process in a biological system.

The paper is organized as follows. We present the detailed theory and procedure of the ID approach in Section 2. In Sec. 4, the numerical efficiency of the ID approach is demonstrated for the Ohmic and subOhmic spectral densities by comparing it with the other methods, and in Sec. 5 the discretization of highly structured spectral densities and the dynamics of the electron transfer in cryptochromes are demonstrated. Conclusions and discussions are reported in Sec. 6.

2 Linear Dissipation in Thermo-field dynamics

2.1 Linear dissipative model

Let us consider a system linearly coupled to a bosonic heat bath with inverse temperature β , which consists of a canonical distribution of harmonic oscillators. The Hamiltonian operator can be written as

$$H = H_S + \sum_k \omega_k a_k^\dagger a_k + V_{SB} \sum_k g_k (a_k^\dagger + a_k). \quad (1)$$

where H_S is a system Hamiltonian and V_{SB} is a system part of a system-bath coupling. $a_k, a_k^\dagger, \omega_k$ and g_k are the annihilation operator, creation operator, frequency, and system-bath coupling constant for the k th mode of the bath, respectively.

From a dynamical point of view, the effect of the bosonic heat bath at an inverse temperature β on the system is exclusively determined by the BCF⁴⁴

$$C(t) = \frac{1}{2\pi} \int_{-\infty}^{\infty} d\omega S_\beta(\omega) e^{-i\omega t}, \quad (2)$$

where we define the quantum noise spectral density (QNSD)⁹

$$S_\beta(\omega) \equiv \frac{1}{2\pi} J(\omega) \left[\coth\left(\frac{\beta\omega}{2}\right) + 1 \right] \quad (3)$$

with $J(\omega) = \sum_k g_k^2 (\delta(\omega - \omega_k) - \delta(\omega + \omega_k))$. In the following, we will refer to Eq. (2) as BCF-QNSD relation. Explicitly writing

$$C(t) = \sum_k \left\{ \frac{g_k^2}{2\pi} \left[\coth\left(\frac{\beta\omega_k}{2}\right) + 1 \right] e^{-i\omega_k t} - \frac{g_k^2}{2\pi} \left[-\coth\left(\frac{\beta\omega_k}{2}\right) + 1 \right] e^{i\omega_k t} \right\}, \quad (4)$$

we can state that when the BCF can be written in the form of Eq. (4), the corresponding dynamical system is described by the Hamiltonian Eq. (1) and the bath is at the inverse temperature β .

2.2 Thermo field dynamics

The latter statement can be transformed into a powerful theoretical and computational tool by exploiting the Thermo field dynamics (TFD) framework. TFD is a methodology that facilitates the treatment of quantum systems at non-zero temperatures using the framework of wavefunction formalism.^{45–47} Here we only briefly review the TFD approach and demonstrate its relation to the Eq. (2).

We first consider the Hamiltonian of bosonic free particles

$$H_B = \sum_k \omega_k a_k^\dagger a_k, \quad (5)$$

and label the eigenstates of the k -th boson as $|n_k\rangle$. Then, we introduce the so-called tilde space, denoted as $|\tilde{n}_k\rangle$, which is the Hilbert space of a fictitious dynamical system identical to the original physical system. Additionally, the tensor product of the physical and tilde spaces is referred to as the twin space.^{46,48} A ket vector in the twin space is given by

$$|m_k, \tilde{n}_k\rangle \equiv |m_k\rangle \otimes |\tilde{n}_k\rangle, \quad (6)$$

from which the identity vector is defined as

$$|I\rangle \equiv \bigotimes_k \sum_{n_k} |n_k, \tilde{n}_k\rangle. \quad (7)$$

Using the canonical distribution operator $\rho_{\text{eq}} = e^{-\beta H_B} / \text{Tr}\{e^{-\beta H_B}\}$ and Eq. 7 the so-called thermal vacuum state is derived

$$|0(\beta)\rangle \equiv \rho_{\text{eq}}^{\frac{1}{2}} |I\rangle \quad (8)$$

$$= \prod_k [1 - e^{-\beta\omega_k}]^{\frac{1}{2}} \exp\left(e^{-\beta\omega_k/2} a_k^\dagger \tilde{a}_k^\dagger\right) |\mathbf{0}\rangle \quad (9)$$

$$= e^{-iG_\theta} |\mathbf{0}\rangle, \quad (10)$$

Here, $|\mathbf{0}\rangle = \bigotimes_k |0_k, \tilde{0}_k\rangle$ represents the vacuum state of the ensemble of physical and tilde bosons, and

$$G_\theta = -i \sum_k \theta_k(\beta) \left(a_k \tilde{a}_k - a_k^\dagger \tilde{a}_k^\dagger \right), \quad \theta_k(\beta) = \text{arctanh}\left(e^{-\beta\omega_k/2}\right). \quad (11)$$

The transformation e^{-iG_θ} is referred to as the thermal Bogoliubov transformation. It is worth noting that the transformation from Eq. (9) to Eq. (10) can be performed using the Baker-Campbell-

Hausdorff formulas for $\text{su}(1, 1)$ Lie algebra.⁴⁹

Let us now consider the case in which the initial density matrix of our model can be represented as the direct product of a pure state of the system $|\psi_e\rangle\langle\psi_e|$, and of the bath density matrix, that is

$$\rho(0) = Z^{-1} |\psi_e\rangle\langle\psi_e| \rho_B. \quad (12)$$

where Z is a properly defined partition function. Under this assumption, it is possible to demonstrate^{6,12,13,50,51} that the expectation value of an arbitrary operator A acting on the Hilbert space of the physical system can be written as

$$\langle A(t) \rangle = \langle \psi_\theta(t) | A_\theta | \psi_\theta(t) \rangle \quad (13)$$

where the wavefunction $|\psi_\theta(t)\rangle$ satisfies the Schrödinger equation

$$i \frac{\partial}{\partial t} |\psi_\theta(t)\rangle = H_\theta |\psi_\theta(t)\rangle, \quad |\psi_\theta(0)\rangle = |\psi_e\rangle \otimes |\mathbf{0}\rangle. \quad (14)$$

with the thermal operators

$$H_\theta = e^{iG} \hat{H} e^{-iG} \quad A_\theta = e^{iG} A e^{-iG}. \quad (15)$$

The modified Hamiltonian operator \hat{H} of Eq. (15) is defined as

$$\hat{H} = H - \tilde{H}_B \quad (16)$$

where $\tilde{H}_B = \sum_k \omega_k \tilde{a}_k^\dagger \tilde{a}_k$ is the free-boson Hamiltonian operator of the bosonic tilde space. The thermal Hamiltonian H_θ controls the finite temperature dynamics and is readily obtained by applying

the Bogoliubov thermal transformation to the Hamiltonian operator of Eq. (16)

$$\begin{aligned}
H_\theta &= e^{iG_\theta} \hat{H} e^{-iG_\theta} \\
&= H_S + \sum_k \omega_k (a_k^\dagger a_k - \tilde{a}_k^\dagger \tilde{a}_k) \\
&\quad + V_{\text{SB}} \sum_k g_k \left\{ (a_k + a_k^\dagger) \cosh(\theta_k) + (\tilde{a}_k + \tilde{a}_k^\dagger) \sinh(\theta_k) \right\}.
\end{aligned} \tag{17}$$

Representing the operators and frequencies of physical space and tilde space with common symbols as

$$\{a_k, \tilde{a}_k\} \rightarrow \{a_k\} \tag{18}$$

$$\{\omega_k, -\omega_k\} \rightarrow \{\omega_k\} \tag{19}$$

$$\{g_k \cosh \theta_k, g_k \sinh \theta_k\} \rightarrow \{g_k(\beta)\}, \tag{20}$$

the TFD Hamiltonian Eq. (17) can be expressed in the simpler form

$$H_\theta = H_S + \sum_k \omega_k a_k^\dagger a_k + V_{\text{SB}} \sum_k g_k(\beta) (a_k + a_k^\dagger). \tag{21}$$

2.3 Connection between TFD and the BCF-QNSD relation

The parameters $g_k \cosh(\theta_k)$ and $g_k \sinh(\theta_k)$ entering the thermal Hamiltonian H_θ govern the coupling of the subsystem with the physical and tilde bosonic DoFs. The SD for the thermal system-bath Hamiltonian Eq. (17) can be written as

$$J_\theta(\omega) = J_p(\omega) + J_t(\omega) \tag{22}$$

where

$$J_p(\omega) \equiv \sum_k (g_k \cosh(\theta_k))^2 \delta(\omega - \omega_k) \Theta(\omega) \quad (23)$$

$$J_t(\omega) \equiv \sum_k (g_k \sinh(\theta_k))^2 \delta(\omega + \omega_k) \Theta(-\omega), \quad (24)$$

where $\Theta(\omega)$ is the Heaviside step function, which describe the system-bath couplings in the physical (subscript p) and tilde (subscript t) subspace, respectively. As the temperature goes to zero, $J_p(\omega) \rightarrow J(\omega)$ and $J_t(\omega) \rightarrow 0$. By making use of the relations

$$\cosh^2(\theta_k) = \frac{1}{2} [\coth(\beta\omega_k/2) + 1] \quad (25)$$

$$\sinh^2(\theta_k) = -\frac{1}{2} [-\coth(\beta\omega_k/2) + 1], \quad (26)$$

we immediately see that Eq. (3) and Eq. (22) are equivalent as

$$J_\theta(\omega) = \pi S_\beta(\omega). \quad (27)$$

Therefore, we have demonstrated that the system-bath Hamiltonian of Eq. (1) at temperature β , and the extended zero temperature Hamiltonian Eq. (17) have the same correlation function and hence the same dynamical behaviour.

Concluding, we can state that whenever the BCF can be written in the form

$$C(t) = \sum_k g_k^2(\beta) e^{-i\omega_k t}, \quad \omega_k, g_k(\beta) \in \mathbb{R}, \quad (28)$$

the system dynamics at temperature β is described by the TFD Hamiltonian of Eq. (21). This is the fundamental principle of our method. Note that the frequencies ω_k can be negative in finite temperature cases, and here we do not perform thermo-field doubling, as in the standard TFD formalism,^{12,51} but instead directly determine a set of temperature-dependent parameters $(\omega_k, g_k(\beta))$.

3 Low-rank discretization

Up to this point, we have discussed two equivalent representations of the linear dissipative model. Our goal is finding an approximation $\bar{C}(t)$ of the BCF of the form of Eq. (28) with the least number of summands possible, providing a requested tolerance ϵ within a specified time interval $[0, T]$. That is, we wish to solve the problem

$$\|C(t) - \bar{C}(t)\|_{\infty} < \epsilon, \quad t \in [0, T] : \quad \tilde{C}(t) = \sum_{k=1}^M g_k^2 e^{-i\omega_k t} \quad (29)$$

with $g_k, \omega_k \in \mathbb{R}$. Rather than computing $C(t)$ and directly solve the above minimization problem we exploit the information contained in the Eq. (2), and reduce its rank by using the Interpolative Decomposition theory. In the following, we present the fundamental theoretical framework and the detailed procedure of our methodology.

3.1 Calculating the frequencies ω_k

3.1.1 Initial discretization of $f(t, \omega)$

We begin by representing Eq. (2) in a form that is suitable for numerical analysis. First, we set a cutoff frequency Ω such that $S_{\beta}(\omega) = 0$ outside the interval $[-\Omega, \Omega]$ and a cutoff time T . Then rewrite Eq. (2) as

$$C(t) = \int_{-\Omega}^{\Omega} d\omega f(t, \omega), \quad t \in [0, T]. \quad (30)$$

where $f(t, \omega) \equiv S_{\beta}(\omega)e^{-i\omega t}$. We now define the sets $\mathbf{T} = \{(t_i)_{i=1}^m\}$ and $\mathbf{\Omega} = \{(\omega_j)_{j=1}^n\}$ where $t_i \in [0, T]$ and $\omega_j \in [-\Omega, \Omega]$, and create a dense rectangular grid $\mathbf{T} \times \mathbf{\Omega}$ on which $f(t, \omega)$ is discretized. In this study, we employ an equispaced fine grid, with $t_i = (i - 1)T/(m - 1)$ and $\omega_j = 2(j - 1)\Omega/(n - 1) - \Omega$ with m, n being two large integers. Then the integral in Eq. (30) can

where \mathbf{B} is an $m \times r$ matrix consisting of r columns selected from \mathbf{A} , where $r \leq n$. These columns are chosen so that they provide a good basis for approximating the entire matrix. \mathbf{P} is a $r \times n$ matrix that contains coefficients such that it approximates \mathbf{A} when multiplied by \mathbf{B} . The columns of \mathbf{P} contain a mixture of 1s and 0s that effectively select the corresponding columns in \mathbf{B} , and the other entries in \mathbf{P} are coefficients that interpolate the remaining columns of \mathbf{A} .

In order to apply ID to our problem, we construct a real matrix $\mathbf{f}_{2m \times n}$ with entries $\text{Re } f(t_i, \omega_j)$ and $\text{Im } f(t_i, \omega_j)$

$$\mathbf{f}_{2m \times n} = \begin{pmatrix} (\text{Re } f(t_i, \omega_j))_{i,j=1}^{m,n} \\ (\text{Im } f(t_i, \omega_j))_{i,j=1}^{m,n} \end{pmatrix} \in \mathbb{R}^{2m \times n} \quad (33)$$

Then we can construct a rank r ID of $\mathbf{f}_{2m \times n}$ as

$$\mathbf{f}_{2m \times n} = \mathbf{B}_{2m \times r} \mathbf{P}_{r \times n} + \mathbf{E}_{2m \times n} \quad (34)$$

where

$$\mathbf{B}_{2m \times r} = \begin{pmatrix} (\text{Re } f(t_i, \omega_k))_{i,k=1}^{m,r} \\ (\text{Im } f(t_i, \omega_k))_{i,k=1}^{m,r} \end{pmatrix} \in \mathbb{R}^{2m \times r} \quad (35)$$

with $\omega_k \in \tilde{\Omega} \subset \Omega$, $\mathbf{P}_{r \times n} \in \mathbb{R}^{r \times n}$, and $\mathbf{E}_{2m \times n} \in \mathbb{R}^{2m \times n}$ is an error matrix with $\|\mathbf{E}_{2m \times n}\| \leq \epsilon$. Eq. (34) is schematically depicted in FIG. 1.

The subset $\tilde{\Omega}$ corresponds to the selected columns in the ID. Entrywise, Eq. (34) can be written as

$$f(t_i, \omega_j) = \sum_{k=1}^r f(t_i, \omega_k) P_{kj} + E'_{ij} \quad (36)$$

where $P_{kj} = (\mathbf{P}_{r \times n})_{kj}$, $\text{Re} E'_{ij} = (\mathbf{E}_{2m \times n})_{ij}$ and $\text{Im} E'_{ij} = (\mathbf{E}_{2m \times n})_{(2i)j}$ are entries of matrices $\mathbf{Z}_{r \times n}$

and $\mathbf{E}_{2m \times n}$. Substituting Eq. (36) into Eq. (31), we obtain

$$\begin{aligned} C(t_i) &= \sum_{j=1}^m \sum_{k=1}^r f(t_i, \omega_k) P_{kj} w_j + \sum_{j=1}^m E'_{ij} w_j + e_i \\ &= \sum_{k=1}^r f(t_i, \omega_k) z_k + e'_i \end{aligned} \quad (37)$$

where $z_k = \sum_j P_{kj} w_j$ and $e'_i = e_i + \sum_{j=1}^m E'_{ij} w_j$.¹ At this stage of the procedure, a specific subset of r frequencies ω_k has been selected out of the initial set $\mathbf{\Omega}$ to represent the discretized bath. The final step involves determining the system-bath coupling parameters $g_k(\beta)$, which requires evaluating the weights, z_k .

3.2 Calculating the coupling strengths $g_k(\beta)$

Let us now define the vector \mathbf{c} that stores the values of the BCF for each sample time

$$\mathbf{c} = \begin{pmatrix} (\text{Re } C(t_i))_{i=1}^m \\ (\text{Im } C(t_i))_{i=1}^m \end{pmatrix} \in \mathbb{R}^{2m}, \quad (38)$$

then, from Eq. (37), the coefficients $\mathbf{z} = (z_k)_{k=1}^r \in \mathbb{R}_+^r$ can be obtained by solving the overdetermined linear system

$$\min_{\mathbf{z}} \|\mathbf{c} - \mathbf{Bz}\|_2^2 \quad \text{s.t.} \quad z_k \geq 0. \quad (39)$$

This problem can be solved using the so-called nonnegative least squares (NNLS) technique.⁵² Finally, we obtain the desired approximation

$$\begin{aligned} \bar{C}(t) &= \sum_{k=1}^M f(t, \omega_k) z_k, \quad z_k > 0 \\ &= \sum_{k=1}^M z_k \mathcal{S}_\beta(\omega_k) e^{-i\omega_k t}, \quad z_k > 0. \end{aligned} \quad (40)$$

¹Note that using a complex matrix for ID, without separating the real and imaginary parts of $f(t, \omega)$, is not feasible. This occurs because the frequencies must be chosen such that the matrix P , which leads to the coefficients z_k , is real.

where, for the Hamiltonian operator to be Hermitian, the weights z_k must be positive. From the approximated BCF Eq. (40), we can construct a temperature-dependent effective Hamiltonian Eq. (21) by setting

$$g_k(\beta) = \sqrt{z_k S_\beta(\omega_k)}. \quad (41)$$

Since the NNLS procedure may result in some z_k to be zero, in the general case $M \leq r$.

The overall accuracy of the method is determined by the accuracy of the ID and of the NNLS. We note that ID induces a pivoting of the columns of \mathbf{f} ; therefore, the M frequencies $\{\omega_k\}$ do not correspond to the first M frequencies of the initial discretization grid, but rather form a special subset of it. The discrete data of $C(t)$ in Eq. (38) for the NNLS procedure can be obtained through numerical integration, which can be combined with interpolation techniques such as spline interpolation or the AAA algorithm.⁵³

3.3 Actual usage of the ID method

The method discussed above can be applied in two different ways: i) setting the threshold ϵ of ID ii) setting the maximum rank of the matrix B in Eq (34). The parameters required as an input are (1) the cutoff frequency Ω , (2) the cutoff time T , (3) the number of points used in the initial discretization, (4) the threshold ϵ or the rank r .

4 Discretization of model spectral densities

As a simple example, we first consider spectral densities in power law form with an exponential cut-off

$$J(\omega) = \pi\alpha\omega_c^{1-s}\omega^s e^{-\omega/\omega_c}, \quad (42)$$

which has been extensively employed to study a variety of open quantum systems.⁵⁴ A heat bath is classified according to the value of the parameter s as Ohmic ($s = 1$), sub-Ohmic ($0 < s < 1$), and super-Ohmic ($s > 1$). In order to assess the performance of our method, we compare it with

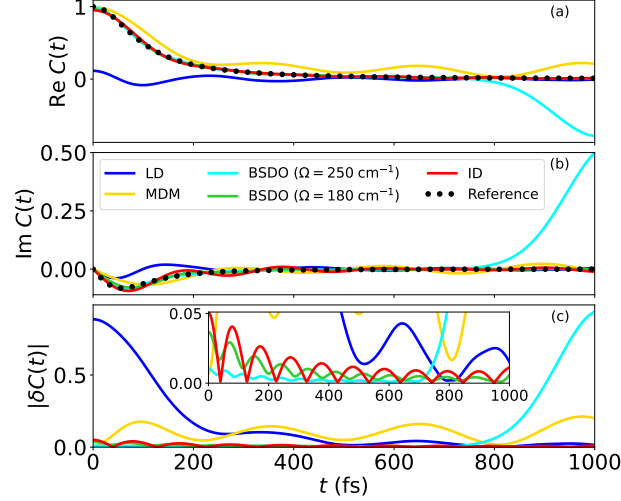


Figure 2: (a) Real part, (b) imaginary part and (c) absolute error of the bath correlation function for the Ohmic spectral density approximated using the LD (blue), MDM (yellow) and ID (red), BSDO for the frequency interval $[-250, 250]$ cm^{-1} (cyan) and $[-180, 180]$ cm^{-1} (green). All the BCFs are approximated with 20 sample points. The absolute error is defined as $|\delta C(t)| = |C_{\text{approx}}(t) - C(t)|$. Black dotted lines are the references. All the results are normalized to the absolute value of $C(0)$.

LD,^{27–29} MDM^{30–32} and BSDO^{33,34} approaches (See Appendix for details). Note that the LD and BSDO approaches are applied to the QNSD, although they were originally developed for the SD, to allow a fair comparison with the ID approach. It should be noted that the BSDO approach for QNSD is equivalent to the thermalized version of the time-evolving density operator with orthogonal polynomials (T-TEDOPA)²⁴ through chain mapping.

For testing population dynamics, we adopt the spin-boson model

$$H = -\Delta\sigma_x + \sum_k \omega_k a_k^\dagger a_k + \sigma_z \sum_k g_k (a_k^\dagger + a_k) \quad (43)$$

where σ_x and σ_z are the Pauli matrices, Δ is the coupling between states. The parameters are fixed to $\omega_c = 53$ cm^{-1} , $\alpha = 5$ and $\Delta = 40$ cm^{-1} . Note that the parameters used in this section are similar to those employed in our previous study on the decomposition of BCFs.⁵⁵ The initial grids for the ID approach comprise 500 points in time domain and 2000 points in frequency domain for all the results in this section. The results obtained using the HEOM approach with the ESPRIT technique for the decomposition of the BCF^{55–58} are also shown in the figures as references.

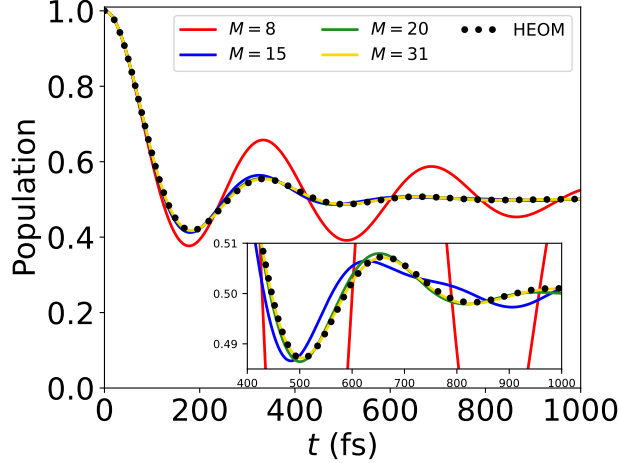


Figure 3: Population dynamics of the first state of the spin-boson model Eq. (43) with the Ohmic spectral density calculated using 8 (red), 15 (blue), 20 (green) and 31 (yellow) bosons obtained using the ID approach. The dotted line is the result calculated using HEOM with the ESPRIT decomposition.

4.1 Ohmic bath

We present the BCF and population dynamics for the Ohmic case ($s = 1$) in FIG. 2 and 3, respectively. The temperature is set to 300 K. The cutoff time and cutoff frequency for the ID approach are $T = 1000$ fs and $\Omega = 500$ cm^{-1} , respectively. The BCF is approximated using 20 sample points, which allow the population dynamics to converge with the ID approach (see FIG. 3). We also present the results obtained using the LD, MDM, and BSDO approaches. For the BSDO method, we provide two results using different frequency intervals. The result obtained for the frequency interval $[-250, 250]$ cm^{-1} is the most accurate at early times, but around $t = 700$ fs, the error starts to increase. In contrast, the interval $[-180, 180]$ cm^{-1} yields less accurate results initially but performs better over the whole time interval. Thus, the performance of the BSDO approach is very sensitive to the choice of the frequency interval, which must be carefully defined. Conversely, the ID approach can automatically determine the optimal frequencies to represent the BCF with a specified accuracy, as long as a sufficiently wide frequency interval is used. If the interval is properly chosen, the ID and BSDO approaches show good performance in approximating the BCF over the entire time range. On the other hand, the LD and MDM approaches return very large errors with 20 sample points and require more than 100 points to achieve comparable accuracy.

See the SM for the details. In FIG. 3, we observe that the dynamics rapidly converge with increasing number of sample points. The BCF calculated using the ID approach with 20 vibrations is already in good agreement with the HEOM result. In contrast, in a previous study,¹² the same dynamics has been calculated using the MD method with 200 sample points.

4.2 Sub-Ohmic bath

In FIG. 4 and 6, we present the BCF and population dynamics for the sub-Ohmic case ($s = 0.25$), respectively. The temperature is set to 50 K. We point out that the sub-Ohmic SD is critical at finite temperature because the integrand of the BCF exhibits a singularity at $\omega = 0$ caused by the Bose-Einstein distribution, which disappears in the zero temperature limit. The cutoff time and cutoff frequency for the ID approach are $T = 1000$ fs and $\Omega = 200$ cm⁻¹, respectively. The BCF is approximated using 20 sample points, which allow the population dynamics to converge with the ID approach (see FIG. 6). The ID approach can accurately approximate the BCF over the entire time range, whereas the other methods fail to achieve comparable accuracy. To investigate the behaviour with the number of sample points increasing, we also show the BCF approximated with 500 sample points in FIG. 5. Even with 500 points, MDM and BSDO approaches cannot give accurate results because of the singularity at $\omega = 0$. This implies that the methods based on orthogonal polynomials, such as T-TEDOPA,^{24,59} fail for this class of QNSDs. Conversely, the ID approach does not suffer from the singularity because it can exploit the temporal information enclosed in the BCF through the NNLS procedure. The LD approach provides a good approximation of the SD only when using a very large number of points – over 500 are needed to match the accuracy that the ID method achieves with just 20 points. In FIG. 6, we can observe that the dynamics rapidly converges as the number of sample points increase, and the result with 13 points is already very accurate. The BCF calculated using the ID approach with 20 vibrations agrees with the HEOM result.

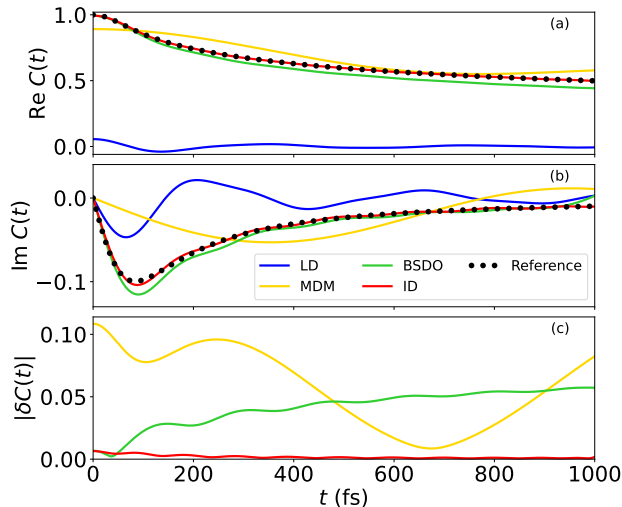


Figure 4: (a) Real part, (b) imaginary part and (c) absolute error of the bath correlation function for the sub-Ohmic spectral density approximated using the LD (blue), MDM (yellow), BSDO (green) and ID (red) with 20 sample points. The absolute error is defined as $|\delta C(t)| = |C_{\text{approx}}(t) - C(t)|$. Black dotted lines are the references. All the results are normalized to the absolute value of $C(0)$.

5 Discretization of structured spectral densities: Electron transfer in biological systems

Complex molecular systems are often characterized by structured spectral densities whose rich features can strongly impact their dynamical behaviour. In order to test the effectiveness of the current method beyond the simple unstructured Ohmic spectral densities, we apply it to determine a low-rank discrete model of the electron-transfer process in plant cryptochromes from *Arabidopsis thaliana* (AtCry). The SD of this process has been obtained from QM/MM simulations with the constrained DFT approach.^{60–62} Using the discretized bath parameters, we also calculate the electron transfer dynamics, and compare it with previous results obtained with the ML-MCTDH method.⁶²

Electron transfer in protein can be modelled using a two-state donor-acceptor model. The

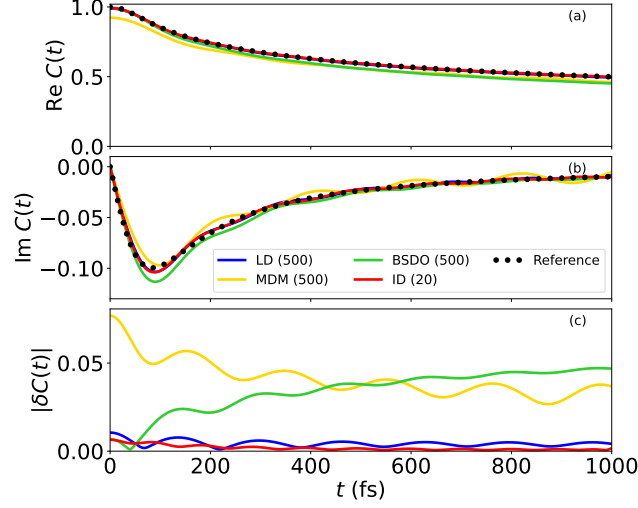


Figure 5: (a) Real part, (b) imaginary part and (c) absolute error of the bath correlation function for the sub-Ohmic spectral density approximated using the LD (blue), MDM (yellow), BSDO (green) and ID (red) with 20 sample points. The absolute error is defined as $|\delta C(t)| = |C_{\text{approx}}(t) - C(t)|$. Black dotted lines are the references. All the results are normalized to the absolute value of $C(0)$.

Hamiltonian is readily written as

$$\begin{aligned}
 H = & H_D |D\rangle\langle D| + H_A |A\rangle\langle A| + H_{DA} (|D\rangle\langle A| + |A\rangle\langle D|) \\
 & + \sum_k \frac{\omega_k}{2} (p_k^2 + x_k^2) + \sum_k g_k x_k (|D\rangle\langle D| - |A\rangle\langle A|),
 \end{aligned} \tag{44}$$

where $|D\rangle$ and $|A\rangle$ denote the donor and acceptor states, respectively. H_D and H_A represent the energies of each state, while H_{DA} denotes the electronic coupling between the donor and acceptor states. Here, x_k , p_k , and ω_k are the position, momentum, and frequency of the k th vibrational mode, respectively. The term g_k represents the vibrational coupling strength of the k th mode, which is related to the displacement g_k/ω_k . This model Hamiltonian assumes that the harmonic potentials in both electronic states have the same frequency, position, and momentum coordinates. We use the parameters $H_D = 0.0$, $H_A = -511.63$ and $H_{DA} = 19.666$ meV, adopted from Ref.⁶² In our model, the reorganization energy is set to 1.34 eV.

Before discretization is performed, we smooth the noise of the SD by employing a smoothing spline to improve the numerical stability of ID. We then apply an interpolation algorithm to the smoothed data to obtain an analytical expression for the spectral density. In this study, we use

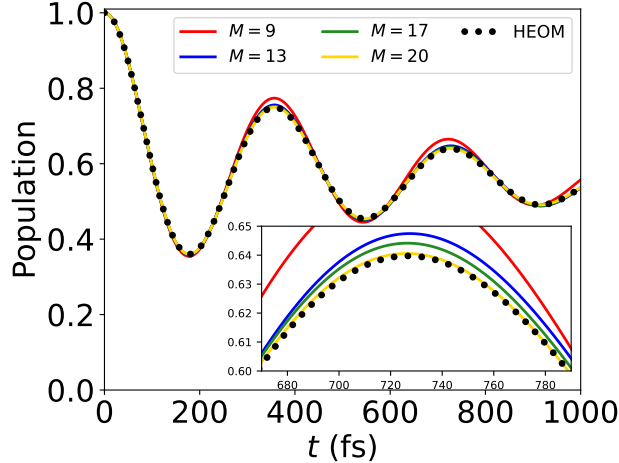


Figure 6: Population dynamics of the first state of the spin-boson model Eq. (43) with the sub-Ohmic spectral density calculated with 9 (red), 13 (blue), 17 (green) and 20 (yellow) bosons obtained using the ID approach. The dotted line is the result calculated using HEOM with the ESPRIT decomposition.

the AAA algorithm. This expression can be used to form the matrix \mathbf{f} and calculate the BCF by numerically integrating Eq. (2). Due to the low reliability of the low frequency part of the spectral density, we set the spectral density to zero for $\omega < 1 \text{ cm}^{-1}$, which is a common practice in the field of electron transfer dynamics.⁶² The spectral density is shown in FIG. 7 (a).

In this section, comparison is only made against the BSDO approach, since it outperforms LD and MDM approaches even in the case of simple SDs, as we have seen in the previous section. For both the ID and BSDO approaches, we consider the frequency interval $[0, 4000] \text{ cm}^{-1}$ unless otherwise specified. The initial grids for the ID approach comprise 1000 points in time domain and 2000 points in frequency domain for all the results in this section.

5.1 Zero temperature

First, we consider the zero-temperature case. In FIG. 7, we present the sample frequencies ω_k and corresponding coefficients g_k^2 obtained using the ID approach with a cutoff time of $T = 250 \text{ fs}$. We observe that the ID approach can effectively capture the characteristic features of the SD. The population dynamics are shown in FIG. 9. The dynamics converge rapidly as the number of sample points increases. The result obtained with 43 vibrations is already in good agreement with the

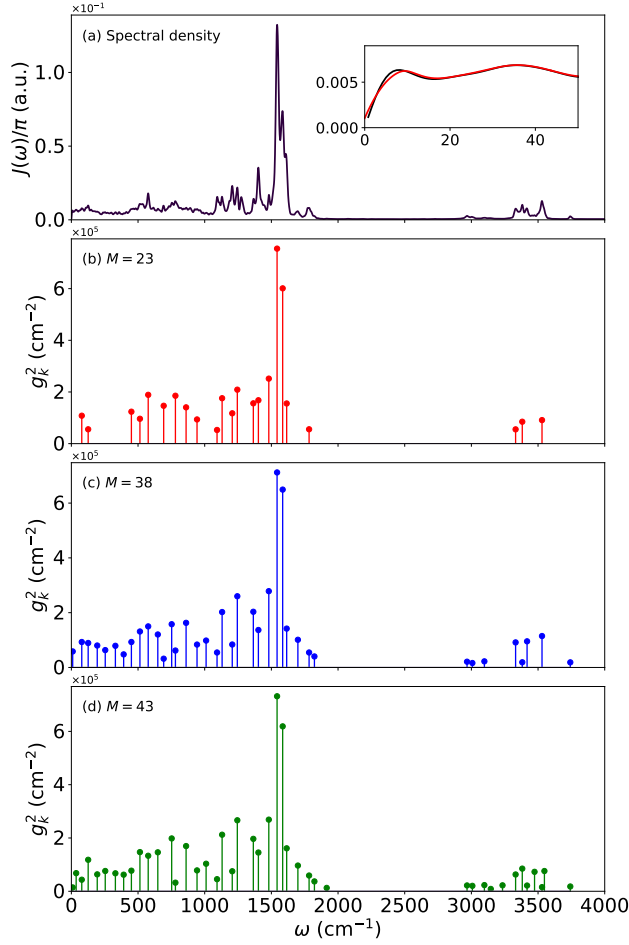


Figure 7: (a) Spectral density $J(\omega)/\pi$ for the cryptochromes (black), coefficients g_k^2 and their corresponding frequencies ω_k of (b) 23, (c) 38 and (d) 43 vibrations obtained using the ID approach with $T = 250$ fs. The inset in (a) shows the low-frequency region of the spectral density, including the original data (black) and the fitted data (red) obtained using the AAA algorithm.

ML-MCTDH result obtained with an equispaced discretization with at least 256 frequencies.⁶² Thus, the ID approach can provide an accurate result using five times fewer sample points. FIG. 8 displays the corresponding BCF with 43 sample points. When we apply the BSDO with the same number of sample points, it yields a more accurate result at early times but starts to deviate from the reference around $t = 200$ fs, and requires 50 sample points to obtain an accurate BCF up to 250 fs.

Next, we consider longer time dynamics to demonstrate the flexibility and robustness of the ID approach. FIG. 10 displays the frequencies ω_k and the corresponding coefficients g_k^2 obtained

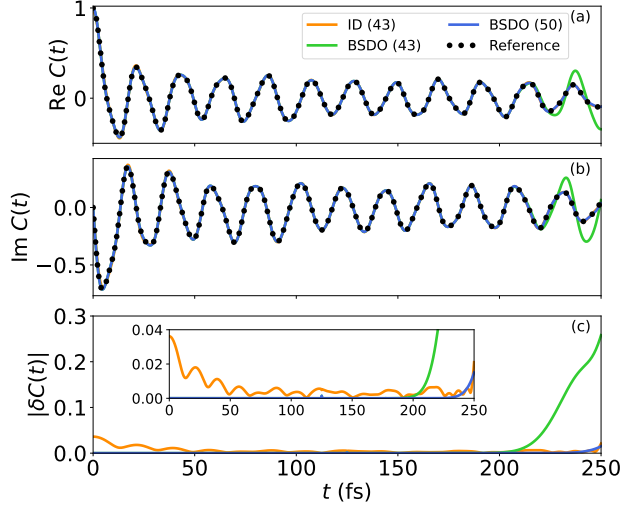


Figure 8: (a) Real part, (b) imaginary part and (c) absolute error of the bath correlation function for the cryptochromes approximated using the ID (red), BSDO with 43 sample points (green) and BSDO with 50 sample points. The absolute error is defined as $|\delta C(t)| = |C_{\text{approx}}(t) - C(t)|$. Black dotted lines are the references. All the results are normalized to the absolute value of $C(0)$.

using the ID approach with $T = 500$ fs. Compared to the discretization obtained using $T = 250$ fs, in this case the sample frequencies are more densely distributed in the low-frequency domain which is expected in order to capture long-time behaviour. As shown in FIG. 12, using the ID approach, the population dynamics converges with 69 vibrational modes. The corresponding BCF is shown in FIG. 11. The BSDO does not yield an accurate BCF over the entire time domain with 69 points and requires nearly 100 sample points to achieve convergence. According to the Lieb-Robinson bound, the number of necessary bath modes required by the BSDO approach can be predicted to increase proportionally with time t , that is, $M \propto t$,³⁴ which agrees well with our current results. In contrast, the ID approach is more robust can capture the long-time behaviour with a smaller number of sample points.

However, we observe that achieving very high accuracy using the ID method is more challenging compared to the BSDO approach. Indeed, our results suggest that the overall accuracy of the ID does not increase significantly despite a greater number of sample points (refer to the SM). Nevertheless, ID consistently demonstrates to be practically reliable for dynamical simulations.

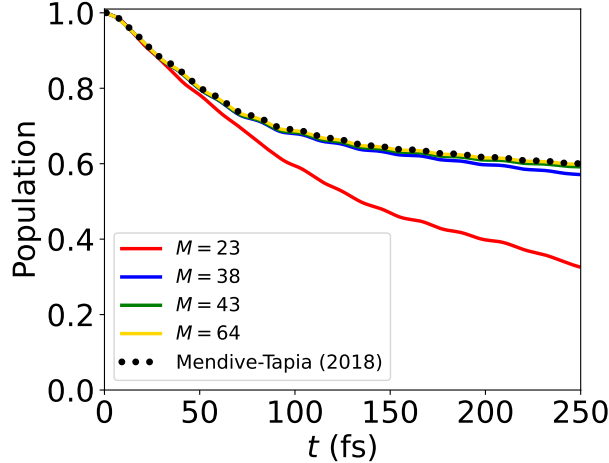


Figure 9: Population dynamics of the donor state at 0 K calculated using 23 (red), 38 (blue), 43 (green) and 64 (yellow) vibrations obtained using the ID approach. The dotted line is the dynamics calculated using ML-MCTDH, taken from Mendive-Tapia et. al. (2018).⁶²

5.2 Finite temperature

Lastly, we test the ID and BSDO approaches for a finite-temperature case at 300 K. The QNSD is shown in FIG. 13 (a). The frequencies ω_k and coefficients g_k^2 obtained using the ID approach with different sample points are also presented in FIG. 13 (b)-(d). The QNSD has a sharp peak around $\omega = 0$ and $\omega = 1500$, and the ID effectively detects these significant frequencies. FIG. 14 and 15 display the BCF and the population dynamics, respectively. Using the ID approach, the population dynamics converges with 59 vibrational modes.

BCFs approximated using the ID and BSDO approaches with 59 sample points exhibit comparable accuracy. However, we found that BSDO results are highly sensitive to the spectral density behavior in the low-frequency region. As previously demonstrated, BSDO can encounter convergence issues with sub-Ohmic spectral densities due to the zero-frequency singularity. At finite temperatures, this issue can originate from the $\coth(\beta\omega/2)$ factor, leading to divergence. In our application, setting the components of $J(\omega)$ below 1 cm^{-1} to zero enabled effective use of BSDO. Additionally, the frequency interval for BSDO was carefully selected as $[-700, 4000] \text{ cm}^{-1}$, as deviations from this range resulted in lower accuracy. By contrast, the ID methodology remains entirely unaffected by such factors.

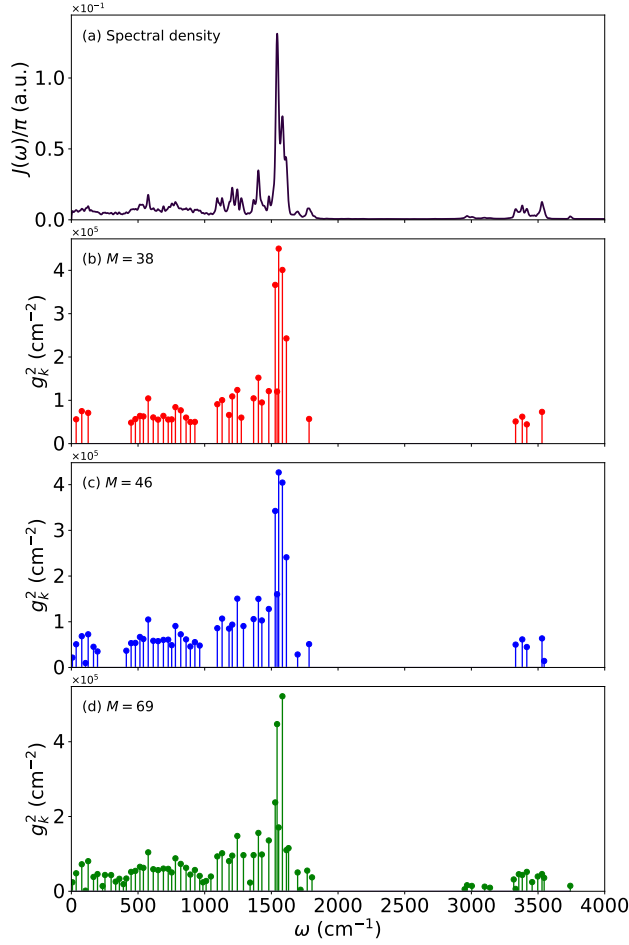


Figure 10: (a) Spectral density $J(\omega)/\pi$ for the cryptochromes (black), coefficients g_k^2 and their corresponding frequencies ω_k of (b) 38, (c) 46 and (d) 69 vibrations using the ID approach with $T = 500$ fs.

In FIG 16, we compare our population dynamics with those calculated in a previous study based on ML-MCTDH and the random phase thermal wave function approach. The populations behave similarly up to $t \approx 100$, fs, after which they start to deviate from each other. Considering that we do not impose any approximations on the dynamics other than the tensor-train ansatz, we conclude that in this system the random phase thermal wave function approach does not properly account for thermal effects.

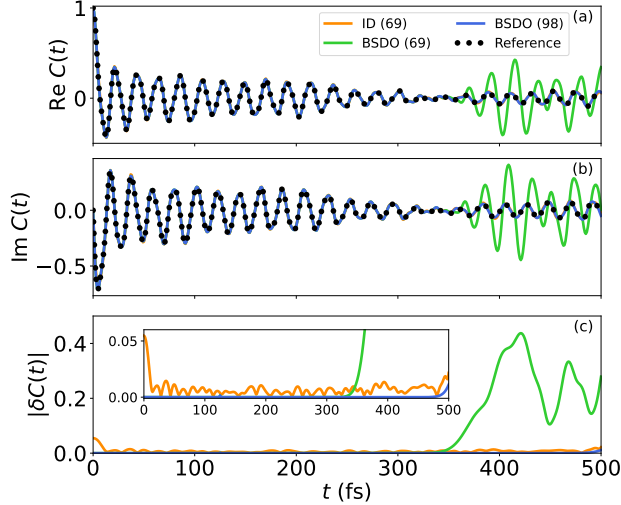


Figure 11: (a) Real part, (b) imaginary part and (c) error of the BCF at 0 K for the cryptochromes approximated using the ID (red), BSDO with 69 sample points (green) and BSDO with 98 sample points (blue). The error is defined as $\delta C(t) = C_{\text{approx}}(t) - C(t)$. Black dotted lines are the references. All the results are normalized to the absolute value of $C(0)$.

6 Discussion and Conclusion

We have proposed a new approach to construct an effective discrete bath Hamiltonian by approximating the BCF using ID theory. Through a comparative analysis with other methodologies, we have shown that the ID approach can both reliably and accurately approximate the BCF using fewer sample points than the alternative techniques.

Two key characteristics distinguish the ID approach from earlier methods. Firstly, it leverages the BCF-QNSD relation and its low-rank decomposition. Additionally, utilizing ID enables the automatic selection of significant frequencies and provides a discrete bath Hamiltonian that incorporates all requisite information for conducting dynamical simulations at a specified level of accuracy. The second characteristic is the emphasis on approximating the BCF instead of directly discretizing the spectral density. The BCF is the key element determining the system’s dynamics. Accurately approximating it is essential for capturing the system’s behavior effectively. Moreover, our method can validate the convergence with respect to the number of sample vibrations by directly assessing the approximation error of the BCF. Modeling ET processes at finite temperature in biological systems is a rather complex problems and can require several hundred vibrations.¹⁴

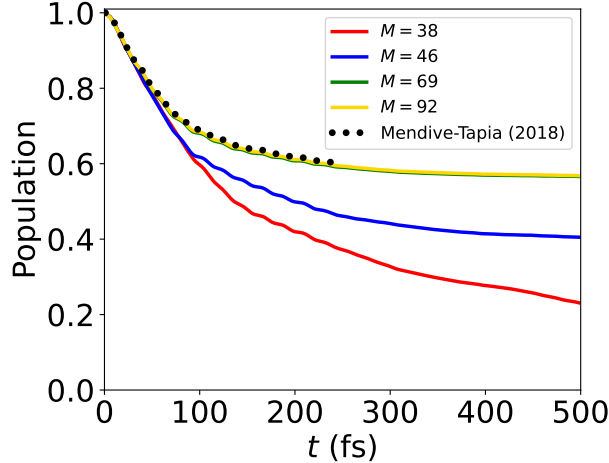


Figure 12: Population dynamics of the donor state at 0 K calculated using 38 (red), 46 (blue), 69 (green) and 92 (yellow) vibrations obtained using the ID approach. The dotted line is the dynamics calculated using ML-MCTDH, taken from Mendive-Tapia et. al. (2018).⁶²

Here, we have demonstrated that our approach can provide converged results with a few tens of sample frequencies.

Through various examples, we have shown that the present method outperforms previous methods in the majority of cases. In some cases, the BSDO method can achieve accuracy comparable to the ID approach. However, for the BSDO method to be effectively utilized, it is essential to properly select the frequency range, which necessitates multiple adjustments through iterative trial-and-error procedures. Furthermore, the BSDO methodology encounters an issue with sub-Ohmic QNSDs due to the Gaussian quadrature weight becoming unbounded at $\omega = 0$. On the other hand, the ID method is more robust and free from these difficulties. Conversely, when the QNSD are not sub-Ohmic, the ID approximation for long-time dynamics can be less accurate than the BSDO.

Finally, we have shown that by integrating this approach with the tensor-train formalism, we can efficiently investigate the quantum dynamics of systems interacting with complex non-Markovian environments. This combination provides reliable and robust computational framework for exploring the dynamics of realistic chemico-physical systems. Although our current study focuses only on bosonic baths, the same techniques can also be effectively applied to fermionic baths. Further research is currently being conducted in this area.

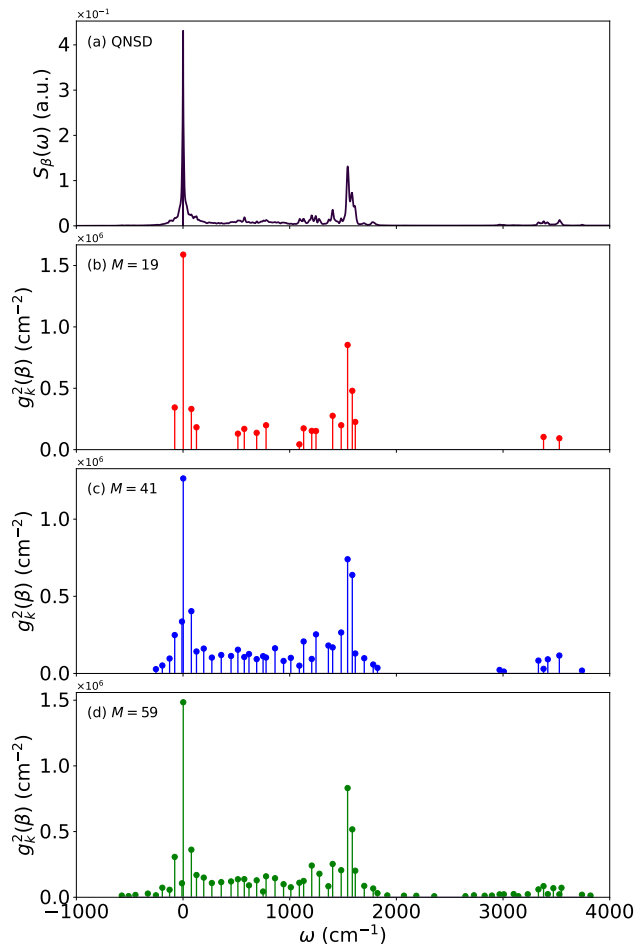


Figure 13: (a) Quantum noise spectral density $S_{\beta}(\omega)$ for the cryptochromes at 300 K (black), coefficients $g_k^2(\beta)$ and their corresponding frequencies ω_k of (b) 11, (c) 41 and (d) 59 vibrations obtained using the ID approach.

Supporting Information Available

The codes used in our simulations are available at the address: <https://github.com/htkhsh/QFiND>.

The supporting information provides additional data.

Acknowledgement

This work has been partially supported by the Spoke 7 "Materials and Molecular Sciences" of ICSC – Centro Nazionale di Ricerca in High-Performance Computing, Big Data and Quantum Computing, funded by the European Union – NextGenerationEU. The authors further acknowledge

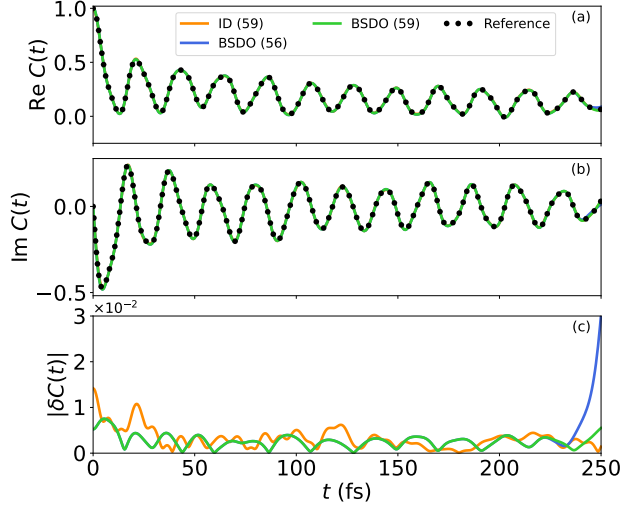


Figure 14: (a) Real part, (b) imaginary part and (c) absolute error of the BCF at 300 K for the cryptochromes approximated using the ID (red), BSDO with 59 sample points (green) and BSDO with 56 sample points (blue). The absolute error is defined as $|\delta C(t)| = |C_{\text{approx}}(t) - C(t)|$. Black dotted lines are the references. All the results are normalized to the absolute value of $C(0)$.

the University of Torino for the local research funding Grant No. BORR-RILO-22-01.

R.B. acknowledges the research project “nuovi Concetti, mAteriali e tecnologie per l’iNtegrazione del fotoVoltAico negli edifici in uno scenario di generazione diffuSa” [CANVAS], funded by the Italian Ministry of the Environment and the Energy Security, through the Research Fund for the Italian Electrical System (type-A call, published on G.U.R.I. n. 192 on 18-08-2022)

A Alternative discretization approaches

We briefly review the discretization methods used for comparison. The problem we consider here is the discretization of $S_\beta(\omega)$ in the frequency interval $[-\Omega, \Omega] \setminus \{0\}$ using M sample frequencies, ω_k ($k = 1, \dots, M$) and the corresponding coefficients $g_k(\beta)$. Some of the methods have been originally developed for the zero-temperature case, and we have adapted them for the finite-temperature case. Note that the order of the frequencies of ω_k is not considered here.

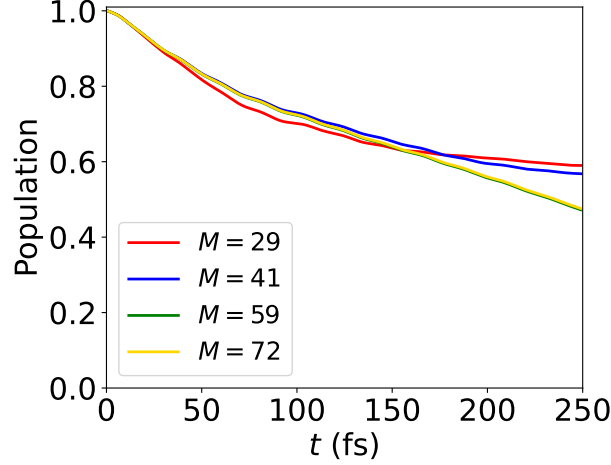


Figure 15: Population dynamics of the donor state at 300 K calculated using 29 (red), 41 (blue), 59 (green) and 72 (yellow) vibrations.

A.1 Logarithmic discretization

The logarithmic discretization is suitable for characterizing the low-frequency domain of the spectral density. We apply this method to positive and negative frequency domains separately. Thus we divide the frequency intervals $[-\Omega, 0)$ and $(0, \Omega]$ into $M - 2$ domains $[-\Lambda^{-(k-1)}\Omega, -\Lambda^{-k}\Omega]$ ($k = 1, \dots, M/2 - 1$) and $[\Lambda^{-(k-M/2)}\Omega, \Lambda^{-(k-1-M/2)}\Omega]$ ($k = M/2 + 1, \dots, M$), respectively. Here we assume that M is even. The parameters ω_k and $g_k(\beta)$ can be obtained as

$$g_k^2(\beta) = \begin{cases} \int_{-\Lambda^{-(k-1)}\Omega}^{-\Lambda^{-k}\Omega} d\omega S_\beta(\omega) & (k = 1, \dots, \frac{M}{2}) \\ \int_{\Lambda^{-k-M/2}\Omega}^{\Lambda^{-(k-1-M/2)}\Omega} d\omega S_\beta(\omega) & (k = \frac{M}{2} + 1, \dots, M) \end{cases} \quad (45)$$

and

$$\omega_k = \begin{cases} g_k^{-2}(\beta) \int_{-\Lambda^{-(k-1)}\Omega}^{-\Lambda^{-k}\Omega} d\omega S_\beta(\omega)\omega & (k = 1, \dots, \frac{M}{2}) \\ g_k^{-2}(\beta) \int_{\Lambda^{-k-M/2}\Omega}^{\Lambda^{-(k-1-M/2)}\Omega} d\omega S_\beta(\omega)\omega & (k = \frac{M}{2} + 1, \dots, M) \end{cases} \quad (46)$$

In this study, we fix the discretization parameter to $\Lambda = 1.1$, which is used in Ref.²⁹

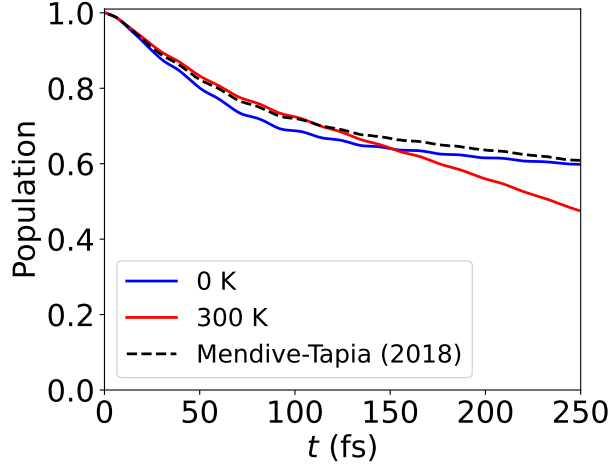


Figure 16: Population dynamics of the donor state at 0K (blue) and 300 K (red). The converged results are presented. The dashed line is the dynamics calculated using ML-MCTDH combined with the random phase thermal wave function approach,⁶³ taken from Mendive-Tapia et. al. (2018).⁶²

A.2 Mode density method

The method by Walters et al.,³² here referred to as the mode density method (MDM), divides the frequency axis into domains with equal weight based on the mode density $\rho(\omega)$ so that each domain has equal renormalization energy. For finite temperatures, we first apply the MDM to the spectral density and obtain the negative frequencies by doubling the obtained sample frequencies. Here, we assume that M is even.

Therefore, the k th sample point should satisfy

$$\int_0^{\omega_k} d\omega \rho(\omega) = k - \frac{1}{2}, \quad (k = 1, \dots, \frac{M}{2}) \quad (47)$$

and

$$\int_0^{\infty} d\omega \rho(\omega) = \frac{M}{2}. \quad (48)$$

Here we employ the mode density

$$\rho(\omega) = \Gamma^{-1} \frac{J(\omega)}{\omega} \quad (49)$$

where Γ is the normalization factor

$$\Gamma = \left(\frac{M}{2}\right)^{-1} \int_0^\infty d\omega \frac{J(\omega)}{\omega}. \quad (50)$$

Then sample frequencies ω_k in the positive domain are determined by solving the nonlinear problem

$$\Gamma^{-1} \int_0^{\omega_k} d\omega \frac{J(\omega)}{\omega} = k - \frac{1}{2}, \quad (k = 1, \dots, \frac{M}{2}), \quad (51)$$

and the negative frequencies are $\omega_{k+M/2} = -\omega_k$. The coefficients are obtained as

$$g_k^2 = \frac{S_\beta(\omega_k)}{\rho(\omega_k)}, \quad (k = 1, \dots, M). \quad (52)$$

A.3 Gauss quadrature with the BSDO weight

BSDO method uses Gauss quadrature to numerically integrate Eq. (2).^{33,34} The unique feature of the BSDO method is that it uses the SD as the weight of a quadrature, enabling to construct an efficient set of polynomial interpolants. In this method, we consider a more general frequency interval $[\Omega_{\min}, \Omega_{\max}]$. Note that the choice of Ω_{\min} and Ω_{\max} affects the accuracy and convergence of the approximation, and it is desirable that the interval covers the entire frequency range of the QNSD i.e. $S_\beta(\omega)$ should be small enough for $\omega < \Omega_{\min}$ and $\omega > \Omega_{\max}$.

We first introduce the so-called hybridization function

$$\Lambda(z) = \int_{\Omega_{\min}}^{\Omega_{\max}} d\omega \frac{S_\beta(\omega)}{z - \omega}, \quad z \in \mathbb{C}. \quad (53)$$

By the Sokhotski-Plemelj theorem, Eq. (53) implies

$$S_\beta(\omega) = -\frac{1}{\pi} \lim_{\epsilon \rightarrow 0^+} \text{Im} \Lambda(\omega + i\epsilon). \quad (54)$$

If $\Lambda(z)$ is approximated with a sum of rational functions as

$$\Lambda(z) \approx \sum_{k=1}^M \frac{g_k^2(\beta)}{z - \omega_k}, \quad (55)$$

the BCF-QNSD relation can be expressed

$$C(t) = -\frac{1}{\pi} \text{Im} \int_{-\infty}^{\infty} d\omega \lim_{\epsilon \rightarrow 0^+} \Lambda(\omega + i\epsilon) e^{-i\omega t} \quad (56)$$

$$= \sum_{k=1}^M g_k^2(\beta) e^{-i\omega_k t}. \quad (57)$$

Thus we consider expressing $\Lambda(z)$ in the form of Eq. (55) using a Gauss quadrature.

To achieve this, we express the integral Eq. (53) in terms of the product of a weight function $w(\omega) \geq 0$ and a function $h(\omega, z)$,

$$\Lambda(z) = \int_{\Omega_{\text{mix}}}^{\Omega_{\text{max}}} d\omega \frac{S_{\beta}(\omega)}{z - \omega} = \int_{\Omega_{\text{mix}}}^{\Omega_{\text{max}}} d\omega w(\omega) h(\omega, z). \quad (58)$$

Now we consider a polynomial interpolant $h_M(\omega, z)$ of $h(\omega, z)$ with degree $M - 1$

$$h(\omega, z) = h_M(\omega, z) + r_M(\omega, z) \quad (59)$$

$$h_M(\omega, z) = \sum_{k=1}^M h(\omega_k, z) l_k(\omega), \quad l_k(\omega_l) = \delta_{kl} \quad (60)$$

where $l_k(\omega)$ can be defined as the $(M - 1)$ -th order polynomial $l_k(\omega) = \prod_{k \neq l} (\omega - \omega_k) / \prod_{l \neq k} (\omega_k - \omega_l)$ and $r_M(\omega, z)$ is a remainder. If choosing the M node points ω_k ,

$$\Lambda(z) = \int_{\Omega_{\text{mix}}}^{\Omega_{\text{max}}} d\omega w(\omega) h(\omega, z) \approx \sum_{k=1}^M W_k h(\omega_k, z) \quad (61)$$

with $W_k = \int_{\Omega_{\text{mix}}}^{\Omega_{\text{max}}} d\omega w(\omega) l_k(\omega)$, which are referred to as Christoffel weights.

In the BSDO approach, the QNSD (originally the SD) is chosen as the weight of the polynomials i.e. $w(\omega) = S_{\beta}(\omega)$ and $h(\omega, z) = \frac{1}{z - \omega}$. The nodes can be determined as the roots of the orthogonal

polynomial $p_M(\omega)$ of degree M , obeying

$$\int_{\Omega_{\text{mix}}}^{\Omega_{\text{max}}} d\omega S_\beta(\omega) p_k(\omega) p_l(\omega) = \delta_{kl}. \quad (62)$$

Such polynomials can be generated using the recurrence relation

$$p_{k+1}(\omega) = (\omega - \alpha_k) p_k(\omega) - \eta_k p_{k-1}(\omega), \quad k = 0, \dots, M-1 \quad (63)$$

where $p_0(\omega) = 1, p_{-1}(\omega) = 0$. α_k and η_k are the recurrence coefficients, which can be obtained, by applying the Lanczos algorithm,^{64–66} as the elements of a tridiagonal matrix

$$\mathbf{A}_M = \begin{pmatrix} \alpha_0 & \sqrt{\eta_1} & 0 & \dots \\ \sqrt{\eta_1} & \alpha_1 & \sqrt{\eta_2} & \ddots \\ 0 & \sqrt{\eta_2} & \alpha_2 & \ddots \\ \vdots & \ddots & \ddots & \ddots \end{pmatrix} \in \mathbb{R}^{M \times M}. \quad (64)$$

By performing an eigenvalue decomposition, $\mathbf{A}_M = \mathbf{U} \text{diag}(\omega_1, \dots, \omega_M) \mathbf{U}^T$, we can obtain the nodes of p_M , leading to sample frequencies ω_k , as the eigenvalues. The Christoffel weights are given by the square of the first element of each eigenvector

$$g_k^2(\beta) = \Delta_w [\mathbf{U}(1, k)]^2 \quad (65)$$

where $\Delta_w = \int_{\Omega_{\text{mix}}}^{\Omega_{\text{max}}} d\omega S_\beta(\omega)$ is the normalization factor.

It is worth remarking that from the matrix \mathbf{A}_M , we can construct the chain representation of the system,^{23,33} which is expressed with the Hamiltonian

$$\begin{aligned} H_{\text{chain}} = & H_S + \sqrt{\Delta_w} V_{\text{SB}} (b_0^\dagger + b_0) + \sum_{k=0}^{M-1} \alpha_k b_k^\dagger b_k \\ & + \sum_{k=0}^{M-2} \sqrt{\eta_k} (b_k^\dagger b_{k+1} + b_k b_{k+1}^\dagger). \end{aligned} \quad (66)$$

where $\{b_k, b_k^\dagger\}$ is a set of bosonic creation and annihilation operators other than the original. This formulation is nothing else but the T-TEDOPA formulation.²⁴

B Tensor-train format

To solve the time-dependent Schrödinger equation Eq. (14) with the Hamiltonian Eq. (21), it is inevitable to utilize effective numerical strategies capable of accurately treating a large number of dynamical variables. In our approach, the TT decomposition, the simplest form of tensor networks, has been adopted. We outline the fundamental concepts of TT decomposition here and show its application in solving the thermal Schrödinger equation. The reader is referred to the original articles for a detailed analysis of the TT theory.⁶⁷

Let us consider a generic state $|\psi\rangle$ of a N dimensional quantum system having the form

$$|\psi\rangle = \sum_{i_1, i_2, \dots, i_N} A(i_1, \dots, i_N) |i_1\rangle |i_2\rangle \cdots |i_N\rangle. \quad (67)$$

where $|i_k\rangle$ labels the basis states of the k -th dynamical variable with n_k states, and the elements $A(i_1, \dots, i_N)$ are complex numbers labeled by N indices and represent a tensor of order N . With the help of the TT format, each element $A(i_1, \dots, i_N)$ of the tensor A is approximated as

$$A(i_1, \dots, i_N) \approx \sum_{\alpha_0, \dots, \alpha_N=1}^{r_0, \dots, r_N} G_{\alpha_0, \alpha_1}^{(1)}(i_1) G_{\alpha_1, \alpha_2}^{(2)}(i_2) \cdots G_{\alpha_{N-1}, \alpha_N}^{(N)}(i_N) \quad (68)$$

where $G^{(k)} \in \mathbb{C}^{r_{k-1} \times n_k \times r_k}$ are tensors of order 3, called cores of the TT decomposition. The dimensions r_k are called compression ranks. Since the product of Equation (41) must be a scalar, the constraint $\alpha_0 = \alpha_N = 1$ must be imposed.

Turning now to the representation of the thermal wavefunction of Eq. (14) in the TT format, we let d be the number of degrees of freedom of the Hamiltonian operator H , and assume that the environment is described using M uncorrelated vibrations. Hence, when we take n_b states for each vibration, the vector $|\psi_\theta(t)\rangle$ of Eq. (14) can be considered as a tensor with $N = d + Mn_b$

indices. Therefore, in Eq. (68) the first d indices label the DoFs of the system, and the remaining Mn_b indices label the bath operators. In Section 4, we solve Eq. (14) using the time-dependent variational principle (TDVP) algorithm⁶⁸ with a compression rank of 70, which is sufficient for convergence. In Section 5, we employ the tAMEn algorithm^{69–71} with a threshold of $\epsilon = 1.0 \times 10^{-3}$, also ensuring convergence.

References

- (1) Oberhofer, H.; Reuter, K.; Blumberger, J. Charge Transport in Molecular Materials: An Assessment of Computational Methods. *Chem. Rev.* **2017**, *117*, 10319–10357.
- (2) Blumberger, J. Recent Advances in the Theory and Molecular Simulation of Biological Electron Transfer Reactions. *Chem. Rev.* **2015**, *115*, 11191–11238.
- (3) Kreisbeck, C.; Kramer, T. Long-Lived Electronic Coherence in Dissipative Exciton Dynamics of Light-Harvesting Complexes. *J. Phys. Chem. Lett.* **2012**, *3*, 2828–2833.
- (4) Schulze, J.; Shibl, M. F.; Al-Marri, M. J.; Kühn, O. Multi-Layer Multi-Configuration Time-Dependent Hartree (ML-MCTDH) Approach to the Correlated Exciton-Vibrational Dynamics in the FMO Complex. *J. Chem. Phys.* **2016**, *144*, 185101.
- (5) Gelin, M. F.; Borrelli, R. Simulation of Nonlinear Femtosecond Signals at Finite Temperature via a Thermo Field Dynamics-Tensor Train Method: General Theory and Application to Time- and Frequency-Resolved Fluorescence of the Fenna–Matthews–Olson Complex. *J. Chem. Theory Comput.* **2021**,
- (6) Borrelli, R.; Gelin, M. F. Simulation of Quantum Dynamics of Excitonic Systems at Finite Temperature: An Efficient Method Based on Thermo Field Dynamics. *Sci. Rep.* **2017**, *7*, 9127.

- (7) Palma, G. M.; Suominen, K.-A.; Ekert, A. K. Quantum Computers and Dissipation. *Proc. Math. Phys. Eng. Sci.* **1996**, *452*, 567–584.
- (8) Kubo, R.; Toda, M.; Hashitsume, N. *Statistical Physics II: Nonequilibrium Statistical Mechanics*, 2nd ed.; Springer Series in Solid-State Sciences, Springer Ser.Solid-State Statistical Physics; Springer-Verlag: Berlin Heidelberg, 1991.
- (9) Clerk, A. A.; Devoret, M. H.; Girvin, S. M.; Marquardt, F.; Schoelkopf, R. J. Introduction to Quantum Noise, Measurement, and Amplification. *Reviews of Modern Physics* **2010**, *82*, 1155–1208.
- (10) Wang, H.; Thoss, M. Multilayer Formulation of the Multiconfiguration Time-Dependent Hartree Theory. *J. Chem. Phys.* **2003**, *119*, 1289–1299.
- (11) Ren, J.; Li, W.; Jiang, T.; Wang, Y.; Shuai, Z. Time-Dependent Density Matrix Renormalization Group Method for Quantum Dynamics in Complex Systems. *WIREs Computational Molecular Science* **2022**, *12*, e1614.
- (12) Borrelli, R.; Gelin, M. F. Quantum Electron-Vibrational Dynamics at Finite Temperature: Thermo Field Dynamics Approach. *J. Chem. Phys.* **2016**, *145*, 224101.
- (13) Borrelli, R.; Gelin, M. F. Finite Temperature Quantum Dynamics of Complex Systems: Integrating Thermo-Field Theories and Tensor-Train Methods. *WIREs Comput. Mol. Sci.* **2021**, *11*, e1539.
- (14) Borrelli, R. Theoretical Study of Charge-Transfer Processes at Finite Temperature Using a Novel Thermal Schrödinger Equation. *Chemical Physics* **2018**, *515*, 236–241.
- (15) Makri, N.; Makarov, D. E. Tensor Propagator for Iterative Quantum Time Evolution of Reduced Density Matrices. I. Theory. *J. Chem. Phys.* **1995**, *102*, 4600–4610.
- (16) Makri, N.; Makarov, D. E. Tensor Propagator for Iterative Quantum Time Evolution of

- Reduced Density Matrices. II. Numerical Methodology. *The Journal of Chemical Physics* **1995**, *102*, 4611–4618.
- (17) Tanimura, Y.; Kubo, R. Time Evolution of a Quantum System in Contact with a Nearly Gaussian-Markoffian Noise Bath. *J. Phys. Soc. Jpn.* **1989**, *58*, 101–114.
- (18) Tanimura, Y. Numerically “Exact” Approach to Open Quantum Dynamics: The Hierarchical Equations of Motion (HEOM). *J. Chem. Phys.* **2020**, *153*, 020901.
- (19) Borrelli, R. Density Matrix Dynamics in Twin-Formulation: An Efficient Methodology Based on Tensor-Train Representation of Reduced Equations of Motion. *J. Chem. Phys.* **2019**, *150*, 234102.
- (20) Cederbaum, L. S.; Gindensperger, E.; Burghardt, I. Short-Time Dynamics Through Conical Intersections in Macrosystems. *Phys. Rev. Lett.* **2005**, *94*, 113003.
- (21) Hughes, K. H.; Christ, C. D.; Burghardt, I. Effective-Mode Representation of Non-Markovian Dynamics: A Hierarchical Approximation of the Spectral Density. II. Application to Environment-Induced Nonadiabatic Dynamics. *J. Chem. Phys.* **2009**, *131*, 124108.
- (22) Hughes, K. H.; Christ, C. D.; Burghardt, I. Effective-Mode Representation of Non-Markovian Dynamics: A Hierarchical Approximation of the Spectral Density. I. Application to Single Surface Dynamics. *J. Chem. Phys.* **2009**, *131*, 024109.
- (23) Prior, J.; Chin, A. W.; Huelga, S. F.; Plenio, M. B. Efficient Simulation of Strong System-Environment Interactions. *Phys. Rev. Lett.* **2010**, *105*, 050404.
- (24) Tamascelli, D.; Smirne, A.; Lim, J.; Huelga, S. F.; Plenio, M. B. Efficient Simulation of Finite-Temperature Open Quantum Systems. *Phys. Rev. Lett.* **2019**, *123*, 090402.
- (25) Hartmann, R.; Werther, M.; Grossmann, F.; Strunz, W. T. Exact Open Quantum System Dynamics: Optimal Frequency vs Time Representation of Bath Correlations. *The Journal of Chemical Physics* **2019**, *150*, 234105.

- (26) Tamura, H.; Martinazzo, R.; Ruckebauer, M.; Burghardt, I. Quantum Dynamics of Ultrafast Charge Transfer at an Oligothiophene-Fullerene Heterojunction. *J. Chem. Phys.* **2012**, *137*, 22A540.
- (27) Bulla, R.; Tong, N.-H.; Vojta, M. Numerical Renormalization Group for Bosonic Systems and Application to the Sub-Ohmic Spin-Boson Model. *Phys. Rev. Lett.* **2003**, *91*, 170601.
- (28) Bulla, R.; Costi, T. A.; Pruschke, T. Numerical Renormalization Group Method for Quantum Impurity Systems. *Rev. Mod. Phys.* **2008**, *80*, 395–450.
- (29) Wang, L.; Chen, L.; Zhou, N.; Zhao, Y. Variational Dynamics of the Sub-Ohmic Spin-Boson Model on the Basis of Multiple Davydov \mathcal{D}_1 States. *J. Chem. Phys.* **2016**, *144*, 024101.
- (30) Makri, N. The Linear Response Approximation and Its Lowest Order Corrections: An Influence Functional Approach. *J. Phys. Chem. B* **1999**, *103*, 2823–2829.
- (31) Wang, H.; Thoss, M.; Miller, W. H. Systematic Convergence in the Dynamical Hybrid Approach for Complex Systems: A Numerically Exact Methodology. *J. Chem. Phys.* **2001**, *115*, 2979.
- (32) Walters, P. L.; Allen, T. C.; Makri, N. Direct Determination of Discrete Harmonic Bath Parameters from Molecular Dynamics Simulations. *J. Comput. Chem.* **2017**, *38*, 110–115.
- (33) de Vega, I.; Schollwöck, U.; Wolf, F. A. How to Discretize a Quantum Bath for Real-Time Evolution. *Phys. Rev. B* **2015**, *92*, 155126.
- (34) Woods, M. P.; Plenio, M. B. Dynamical Error Bounds for Continuum Discretisation via Gauss Quadrature Rules—A Lieb-Robinson Bound Approach. *Journal of Mathematical Physics* **2016**, *57*, 022105.
- (35) Takahashi, H.; Borrelli, R. Effective Modeling of Open Quantum Systems by Low-rank Discretization of Structured Environments. 2024.

- (36) Otsuki, J.; Ohzeki, M.; Shinaoka, H.; Yoshimi, K. Sparse Modeling Approach to Analytical Continuation of Imaginary-Time Quantum Monte Carlo Data. *Physical Review E* **2017**, *95*, 061302.
- (37) Shinaoka, H.; Otsuki, J.; Ohzeki, M.; Yoshimi, K. Compressing Green's Function Using Intermediate Representation between Imaginary-Time and Real-Frequency Domains. *Phys. Rev. B* **2017**, *96*, 035147.
- (38) Kaye, J.; Chen, K.; Parcollet, O. Discrete Lehmann Representation of Imaginary Time Green's Functions. *Phys. Rev. B* **2022**, *105*, 235115.
- (39) Kaye, J.; Chen, K.; Strand, H. U. R. Libdlr: Efficient Imaginary Time Calculations Using the Discrete Lehmann Representation. *Computer Physics Communications* **2022**, *280*, 108458.
- (40) Cheng, H.; Gimbutas, Z.; Martinsson, P. G.; Rokhlin, V. On the Compression of Low Rank Matrices. *SIAM J. Sci. Comput.* **2005**, *26*, 1389–1404.
- (41) Liberty, E.; Woolfe, F.; Martinsson, P.-G.; Rokhlin, V.; Tygert, M. Randomized Algorithms for the Low-Rank Approximation of Matrices. *Proc. Natl. Acad. Sci.* **2007**, *104*, 20167–20172.
- (42) Woolfe, F.; Liberty, E.; Rokhlin, V.; Tygert, M. A Fast Randomized Algorithm for the Approximation of Matrices. *Applied and Computational Harmonic Analysis* **2008**, *25*, 335–366.
- (43) Halko, N.; Martinsson, P. G.; Tropp, J. A. Finding Structure with Randomness: Probabilistic Algorithms for Constructing Approximate Matrix Decompositions. *SIAM Review* **2011**, *53*, 217–288.
- (44) Weiss, U. *Quantum Dissipative Systems*, 4th ed.; WORLD SCIENTIFIC, 2012.
- (45) Umezawa, H.; Matsumoto, H.; Tachiki, M. *Thermo Field Dynamics and Condensed States*; North-Holland: Netherlands, 1982.

- (46) Suzuki, M. Density Matrix Formalism, Double-Space and Thermo Field Dynamics in Non-Equilibrium Dissipative Systems. *Int. J. Mod. Phys. B* **1991**, *05*, 1821–1842.
- (47) Takahashi, Y.; Umezawa, H. Thermo Field Dynamics. *Int. J. Mod. Phys. B* **1996**, *10*, 1755–1805.
- (48) Schmutz, M. Real-Time Green's Functions in Many Body Problems. *Z Physik B* **1978**, *30*, 97–106.
- (49) Ban, M. Decomposition Formulas for $Su(1, 1)$ and $Su(2)$ Lie Algebras and Their Applications in Quantum Optics. *JOSA B* **1993**, *10*, 1347–1359.
- (50) Gelin Maxim F.; Borrelli Raffaele Thermal Schrödinger Equation: Efficient Tool for Simulation of Many-Body Quantum Dynamics at Finite Temperature. *Annalen der Physik* **2017**, *529*, 1700200.
- (51) de Vega, I.; Bañuls, M.-C. Thermofield-Based Chain-Mapping Approach for Open Quantum Systems. *Phys. Rev. A* **2015**, *92*, 052116.
- (52) Lawson, C. L.; Hanson, R. J. *Solving Least Squares Problems*; Society for Industrial and Applied Mathematics, 1974.
- (53) Nakatsukasa, Y.; Sète, O.; Trefethen, L. N. The AAA Algorithm for Rational Approximation. *SIAM J. Sci. Comput.* **2018**, *40*, A1494–A1522.
- (54) Leggett, A. J.; Chakravarty, S.; Dorsey, A. T.; Fisher, M. P.; Zwerger, W. Dynamics of the Dissipative Two-State System. *Rev. Mod. Phys.* **1987**, *59*, 1–85.
- (55) Takahashi, H.; Rudge, S.; Kaspar, C.; Thoss, M.; Borrelli, R. High Accuracy Exponential Decomposition of Bath Correlation Functions for Arbitrary and Structured Spectral Densities: Emerging Methodologies and New Approaches. *The Journal of Chemical Physics* **2024**, *160*, 204105.

- (56) Takahashi, H.; Borrelli, R.; Gelin, M. F.; Chen, L. Finite Temperature Dynamics in a Polarized Sub-Ohmic Heat Bath: A Hierarchical Equations of Motion-Tensor Train Study. *The Journal of Chemical Physics* **2024**, *160*, 164106.
- (57) Roy, R.; Kailath, T. ESPRIT-estimation of Signal Parameters via Rotational Invariance Techniques. *IEEE Transactions on Acoustics, Speech, and Signal Processing* **1989**, *37*, 984–995.
- (58) Pichot, R.; Watson, R. L.; Norton, I. T. Phospholipids at the Interface: Current Trends and Challenges. *Int J Mol Sci* **2013**, *14*, 11767–11794.
- (59) Riva, A.; Tamascelli, D.; Dunnett, A. J.; Chin, A. W. Thermal Cycle and Polaron Formation in Structured Bosonic Environments. *Physical Review B* **2023**, *108*, 195138.
- (60) Řezáč, J.; Lévy, B.; Demachy, I.; De La Lande, A. Robust and Efficient Constrained DFT Molecular Dynamics Approach for Biochemical Modeling. *Journal of Chemical Theory and Computation* **2012**, *8*, 418–427.
- (61) Firmino, T.; Mangaud, E.; Cailliez, F.; Devolder, A.; Mendive-Tapia, D.; Gatti, F.; Meier, C.; Desouter-Lecomte, M.; de la Lande, A. Quantum Effects in Ultrafast Electron Transfers within Cryptochromes. *Phys. Chem. Chem. Phys.* **2016**, *18*, 21442–21457.
- (62) Mendive-Tapia, D.; Mangaud, E.; Firmino, T.; de la Lande, A.; Desouter-Lecomte, M.; Meyer, H.-D.; Gatti, F. Multidimensional Quantum Mechanical Modeling of Electron Transfer and Electronic Coherence in Plant Cryptochromes: The Role of Initial Bath Conditions. *J. Phys. Chem. B* **2018**, *122*, 126–136.
- (63) Nest, M.; Kosloff, R. Quantum Dynamical Treatment of Inelastic Scattering of Atoms at a Surface at Finite Temperature: The Random Phase Thermal Wave Function Approach. *J. Chem. Phys.* **2007**, *127*, 134711.
- (64) Gragg, W. B.; Harrod, W. J. The Numerically Stable Reconstruction of Jacobi Matrices from Spectral Data. *Numerische Mathematik* **1984**, *44*, 317–335.

- (65) Gautschi, W. Algorithm 726: ORTHPOL—a Package of Routines for Generating Orthogonal Polynomials and Gauss-type Quadrature Rules. *ACM Trans. Math. Softw.* **1994**, *20*, 21–62.
- (66) Gautschi, W. Orthogonal Polynomials (in Matlab). *Journal of Computational and Applied Mathematics* **2005**, *178*, 215–234.
- (67) Oseledets, I. Tensor-Train Decomposition. *SIAM J. Sci. Comput.* **2011**, *33*, 2295–2317.
- (68) Lubich, C.; Oseledets, I.; Vandereycken, B. Time Integration of Tensor Trains. *SIAM J. Numer. Anal.* **2015**, *53*, 917–941.
- (69) Dolgov, S. V. A Tensor Decomposition Algorithm for Large ODEs with Conservation Laws. *Comput. Methods Appl. Math.* **2019**, *19*, 23–38.
- (70) Borrelli, R.; Dolgov, S. Expanding the Range of Hierarchical Equations of Motion by Tensor-Train Implementation. *J. Phys. Chem. B* **2021**, *125*, 5397–5407.
- (71) Takahashi, H.; Borrelli, R. Tensor-Train Format Hierarchical Equations of Motion Formalism: Charge Transfer in Organic Semiconductors via Dissipative Holstein Models. *Journal of Chemical Theory and Computation* **2024**, *20*, 7052–7064.

TOC Graphic

Insert graphical abstract.

